CO2–CO capture and kinetic analyses of sodium cobaltate under various partial pressures

CO_2-CO capture and kinetic analyses of sodium cobaltate under various partial pressures

Elizabeth Vera,[1,2] Susana García,[2] M. Mercedes Maroto-Valer,[2] and Heriberto Pfeiffer[1,*]

[1]*Laboratorio de Fisicoquímica y Reactividad de Superficies (LaFReS), Instituto de Investigaciones en Materiales, Universidad Nacional Autónoma de México, Circuito exterior s/n, Ciudad Universitaria, Del. Coyoacán C.P. 04510, Ciudad de México, Mexico.*

[2]*Research Centre for Carbon Solutions (RCCS), Heriot-Watt University, Edinburgh, EH14 4AS, United Kingdom.*

**Corresponding author. Phone +52 (55) 5622 4627, fax +52 (55) 5616 1371 and E-mail pfeiffer@materiales.unam.mx*

Abstract

Sodium cobaltate and some Fe-containing samples were evaluated on the CO, CO_2 and CO-CO_2 sorption at high temperatures and low CO_2 partial pressures, in the presence and absence of oxygen. Initially, CO_2 chemisorption on these samples was analyzed using different P_{CO2}. Results indicated that all the samples were able to chemisorb CO_2 (if $P_{CO2} \geq 0.2$), where Fe-containing $NaCoO_2$ samples clearly showed higher CO_2 chemisorption efficiencies than pristine $NaCoO_2$. These results were explained by the partial iron reduction and the consequent oxygen release. When oxygen was added the chemisorption process was improved as a result of an iron reduction-oxidation mechanism. These results were confirmed kinetically by the Jander-Zhang and Eyring models. The temperature for complete CO catalytic conversion was shifted to lower temperatures as a function of iron content. Finally, simultaneous CO_2 and CO sorption as well as catalytic experiments were tested (in absence or presence of O_2). These results showed that CO was mainly oxidized and chemically captured, over the CO_2 direct capture, in oxygen absence and presence. Iron is able to release and capture oxygen by reduction-oxidation effect and facilitates oxygen dissociation for the carbonation process, through the Mars van Krevelen reaction mechanism.

Keywords: CO_2 chemisorption; CO oxidation; sodium cobaltate; catalysis; kinetics; thermogravimetric analysis; Jander-Zhang model.

1. Introduction

In the last decades, different materials have been proposed as CO_2 sorbents (Wang et al. 2014; Webley 2014; Bhatta et al. 2015). Among them, alkaline ceramics present good properties at high temperatures, where most of these studies analyze the CO_2 sorption process varying temperature, sample chemical composition and/or microstructural modifications or the addition of other chemical elements or compounds, trying to improve one or more CO_2 capture properties (Izquierdo et al. 2018). However, these analyses are usually performed using a saturated CO_2 atmosphere ($P_{CO2} = 1$), although CO_2 partial pressure on real capture gas systems is far from saturated conditions.

Combustion gases usually contain CO_2 partial pressures between 0.1 and 0.2, where CO_2 is mixed with many other active and inert gases (Kenarsai et al. 2013; Wai 2016; Dou et al. 2016). Based on that, CO_2 capture analysis on alkaline ceramics using low P_{CO2} is an important issue. Within this context, in the last years some authors have tested some alkaline ceramics varying this important physicochemical condition (Kaniwa et al. 2017; Kaniwa et al. 2018; Ochoa-Fernandez 2009; Oh-Ishi et al. 2014; Zhang et al. 2017; Zhang et al. 2018; Lara-García and Pfeiffer 2017; Izquierdo et al. 2018). For example, Kaniwa et al. (2017) analyzed the CO_2 chemisorption on lithium orthosilicate (Li_4SiO_4), where CO_2 capture decreased as a function of P_{CO2}, determining the Ellingham diagram for this reaction process. Results fitted very well at P_{CO2} close to 1, but an important deviation was obtained at low P_{CO2}. However, when Li_4SiO_4 with smaller particle size was analyzed this deviation was reduced, indicating that CO_2 capture process highly depends on kinetics. In a different work, Oh-Ishi et al. (2014) compared reactivity of CO_2 with Li_2CuO_2 and Li_4SiO_4 using different P_{CO2}. Kinetically, Li_2CuO_2 and Li_4SiO_4 did not show any significant variations at $T \leq 660$

°C, but at higher temperatures Li_2CuO_2 presented a superior kinetic behavior than that of Li_4SiO_4, independently of P_{CO2}. In fact, Li_2CuO_2 did not present significant CO_2 capture decrements at low P_{CO2}, while Li_4SiO_4 decreased its CO_2 capture capacity in more than 90 %.

On the other hand, the use of a CO_2 saturated atmosphere implies that some oxygen atoms present on the alkaline ceramic crystal structure must be released to produce the corresponding carbonate (Li_2CO_3 or Na_2CO_3) (Bhatta et al. 205; Lara-García et al. 2017; Izquierdo et al. 2018). Therefore, oxygen diffusion and reactivity are importantly involved on CO_2 chemisorption in this kind of ceramics. Finally, the sorption competition of different gases is an important issue that must be taken into account for gas separation systems (Webley 2014; Regufe et al. 2018; Yañez-Aulestia et al. 2018). For example, Yañez-Aulestia et al. (2018) showed that although CO and CO_2 compete for their sorption on lithium cuprate, CO is preferentially chemisorbed. All these results clearly showed that oxygen diffusion, release and reactivity are important factors during alkaline ceramic carbonation processes.

Based on the aforementioned studies, recent works have reported the use of alkaline ceramics for CO oxidation and subsequent CO_2 chemisorption (Vera et al. 2015; Vera et al. 2016; Alcántar-Vázquez et al. 2016; Lara-García et al. 2017; Vera et al. 2018). For example, it has been probed that Li_5FeO_4 is able to oxidize CO to CO_2 and then trap it chemically, in the presence or even absence of oxygen. This reaction process may be used for developing new gas separation systems on biogas, syngas or other processes (Stonor et al. 2015; Zhao et al. 2018). For example, there are different syngas or biogas effluents containing CO-CO_2 mixtures, in addition to other gases such as methane and/or hydrogen (Stonor et al. 2015), where the carbon oxides sorption and/or separation separations are ideally desired. Finally,

pristine sodium cobaltate ($NaCoO_2$) and other transition metal-containing materials (Fe-, Cu- and Ni-$NaCoO_2$) have been recently proposed as new CO_2 or CO oxidant and subsequent CO_2 chemisorbents (Vera et al. 2018; Vera et al. 2015; Vera et al. 2016). In this context, $NaCoO_2$ has shown different interesting properties during CO_2 chemisorption, always performed with $P_{CO2} = 1$. Based on that, the aim of the present work was to study, through dynamic and isothermal thermogravimetric and catalytic analyses, the CO_2 and CO chemisorption of pristine $NaCoO_2$ and Fe-containing $NaCoO_2$ samples under different partial pressures, in absence or presence of oxygen.

2. Experimental section

Pristine sodium cobaltate and iron-containing sodium cobaltate samples were synthesized by solid-state reaction using sodium carbonate (Na_2CO_3, J. T. Baker), cobalt carbonate ($CoCO_3$, Aldrich) and iron oxide (Fe_2O_3, Meyer) as reagents. The corresponding amounts of each reagent were mechanically mixed and the resulting powder was calcined at 850 °C for 12 h to synthesize $NaCo_{1-x}Fe_xO_2$, where the Fe/Co mole contents were x = 0, 0.1, 0.2 and 0.3. These samples were labeled as $NaCoO_2$, Fe10, Fe20 and Fe30, respectively. The reproducibility of the synthesis was verified more than twice. Then, samples were characterized by powder X-ray diffraction to confirm the sodium cobaltate production. The crystal identification of the samples was performed using different Powder Diffraction Files (PDF) reported on literature. Additionally, Fe-containing $NaCoO_2$ microstructures were analyzed by scanning electron microscopy using a JEOL JMS-7600F.

CO_2 chemisorption was performed in a thermogravimetric balance (Q500HR, TA Instruments) by dynamic and isothermal analyses. The experiments were carried out using a total flow of 60 mL/min with different CO_2 partial pressures (Praxair grade 3) in presence or absence of O_2 (Praxair, grade 2.4), diluted in N_2 (Praxair grade 4.8). Initially, samples were dynamically heated from 30 to 900 °C at 5 °C/min. Then, isothermal experiments were performed only with the Fe30 sample, heating the sample in N_2 up to the desired temperature and then changing the flow to the CO_2-O_2-N_2 mixture.

CO oxidation and subsequent CO_2 chemisorption experiments were performed and evaluated in a catalytic reactor as well as in a thermogravimetric balance. In the catalytic reactor (Bel-Rea, from Bel Japan) 200 mg of sample were used with a gas mixture of 5 vol% O_2, 5 vol% CO and N_2 as balance, using a total flow of 60 mL/min. These volumes were selected in order to have a molar relation $CO/O_2 = 1$, which guarantees that CO oxidation takes place. Gas products were analyzed in a GC-2014 gas chromatograph, from Shimadzu, using a Carboxen-1000 column. Two types of experiments were carried out, dynamic and isothermal. In dynamic analysis, samples were heated from 30 to 900 °C at 5 °C/min. Then, for isothermal analysis, samples were heated up to the desired temperature in N_2 (300 to 800 °C, each 100 °C) at a heating rate of 15 °C/min and exposed to CO-O_2 gas flow for 3 hours. Some isothermal products were further characterized by XRD. Finally, CO_2 chemisorption, produced after the CO oxidation, was determined in a Q500HR thermobalance (TA Instruments). Dynamic and isothermal experiments were carried out using similar conditions than those utilized in the catalytic reactor. Finally, different sorption experiments with CO-CO_2 or CO-CO_2-O_2 N_2 balanced to 60 mL flows were performed following the same procedure used for CO catalytic and sorption analysis described above.

3. Results and Discussion

3.1 Synthesis and characterization

XRD patterns of all the synthesized compounds were identified with the 01-087-0274 PDF file database corresponding to $Na_{0.74}CoO_2$ hexagonal phase (supplementary information, Figure S1). Additionally, the presence of $NaFeO_2$ (01-076-2299 PDF) and FeO (99-101-0507 PDF) were evident on 20 and 30 mol% Fe-content samples, making composites materials in those cases. Backscattered electron images of Fe-containing $NaCoO_2$ are shown in Figure 1. Samples formed polyhedral flat flake-like particles. Particle sizes varied from 1 to 10 μm, where the smallest particles were located at the surface. Besides, they presented an initial slightly carbonation (dark phase), possibly corresponding to Na_2CO_3. Energy dispersive spectroscopy (EDS) showed that iron is homogenously dispersed in all samples, although tiny superficial particles seem to contain more iron, which may correspond to $NaFeO_2$ or FeO phases previously detected by XRD. Therefore, while part of Fe is incorporated into the structure of $NaCoO_2$, another significant part is located on the particle surface.

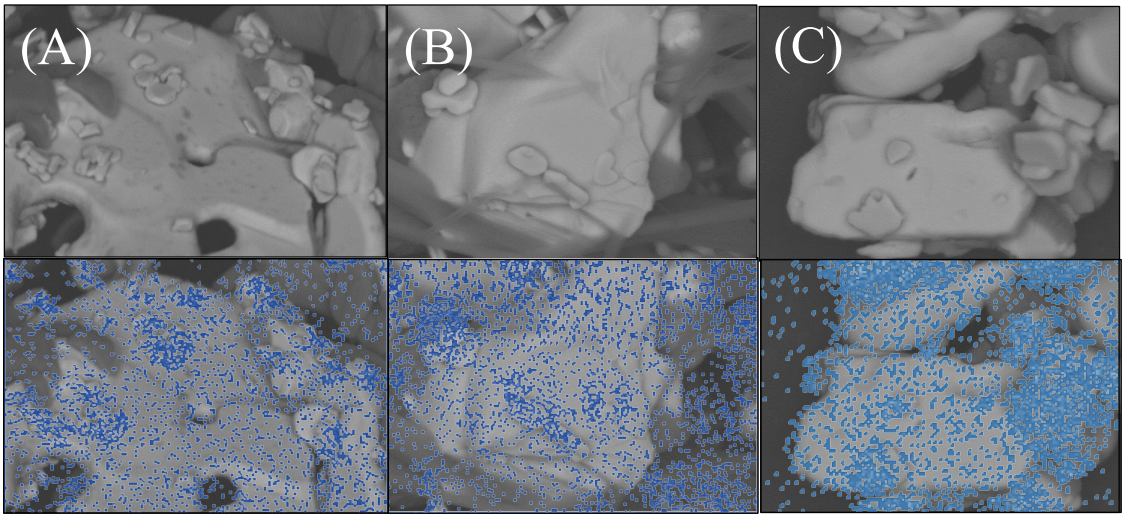

Figure 1. Backscattered electron images and iron EDS mapping distribution on Fe10-$NaCoO_2$ (A), Fe20-$NaCoO_2$ (B), Fe30-$NaCoO_2$ (C).

3.2 CO_2 capture in presence of low CO_2 and O_2 partial pressures

As previously mentioned, a recent study showed that Fe-containing $NaCoO_2$ presents an improved CO_2 chemisorption behavior compared to $NaCoO_2$ (Vera et al. 2018). However, these results were obtained using a saturated atmosphere. Therefore, in this work, the use of different partial pressures is presented and analyzed. Since Fe30 showed the highest CO_2 sorption capacities (Vera et al. 2018), first analyses on the effect of low CO_2 partial pressures (P_{CO2}) were performed with this sample. Figure 2-A presents the results from TG analyses performed on this sample and using five different P_{CO2} (0.05, 0.1, 0.2, 0.3 and 0.8). In general, trends followed similar behaviors to previous ones reported for other alkaline ceramics (Zhang et al. 2018; Lara-García et al. 2017; Kenarsari et al. 2013), where superficial and bulk chemisorption stages are identified. These materials present, initially, a CO_2 superficial chemisorption, producing and external shell composed by the corresponding alkaline carbonate (Na_2CO_3, in this case) and secondary phases. After that, different diffusion

processes must be activated in order to continue the CO_2 chemisorption on the ceramic bulk. Of course, all these phenomena produces limitations and changes in the reaction kinetics [Zhang 2019]. In this case, Fe30-$NaCoO_2$ presents a continuous weight increase from 100 to 805 °C. This weight increment can be attributed to $NaCoO_2$ superficial and bulk CO_2 chemisorption, as well as to an enhanced CO_2 capture produced by Fe and Co reductions (Vera et al. 2018), which implies an oxygen release. It must be pointed out that CO_2 capture capacities were modified under different P_{CO2} values, which also affected the maximum weight increments and chemisorption temperatures. CO_2 maximum chemisorption, using a P_{CO2} of 0.8, was 8.2 wt% and it was produced at 805 °C. Then, and as it would be expected, CO_2 chemisorption is lower as P_{CO2} decreases, ranging from 7.3 to 5 wt% at 0.3 to 0.05 P_{CO2}, respectively. Moreover, desorption temperature was shifted to lower values when P_{CO2} decreased, from 805 to 765 °C when P_{CO2} changed from 0.3 to 0.05. Even in the P_{CO2} = 0.05 case, the desorption processes reached different equilibriums due to the solid-gas interface concentration. This finding follows previously reported trends, where inversion temperatures for different sorbents are reported for different P_{CO2} (Chowdhury et al. 2013). This behavior is quite relevant for the integration of sorbents in plants, as it implies a less-energy-intensive regeneration-step. As it can be seen, weight uptake differences for experiments under P_{CO2} between 0.1 and 0.3 are negligible. Therefore, the following experiments were performed using only a P_{CO2} of 0.2 to evaluate the effect of a non-saturated P_{CO2} in the chemisorption process on Fe30-$NaCoO_2$.

The Fe concentration effect during CO_2 chemisorption was studied (Figure 2-B). As in a saturated atmosphere, Fe-containing samples showed a higher CO_2 chemisorption under a P_{CO2} of 0.2 than that of pristine $NaCoO_2$. These samples presented continuous weight

increments, as in the previous case, where the maximum weight uptakes varied from 7.2 to 4.1 wt% for Fe30 and Fe10, respectively, while pristine $NaCoO_2$ only presented a maximum weight increment of 3.3 wt%. Additionally, it can be seen that the weight increase slope, between 600 and 780 °C, is greater for Fe20 sample (0.02314 wt%/°C) than those of Fe30 and Fe10 (both present a very similar slope; 0.01682 wt%/°C). This effect can be associated to iron availability on $NaCoO_2$ particle surface. It has been reported that iron concentration is mainly located on Fe20 particle surfaces (Vera et al. 2018), while on Fe10 and Fe30 iron atoms are incorporated mainly into the $NaCoO_2$ structure. In the Fe10 case, iron reduction might be hindered, as well as its capacity to dissociate oxygen, leading to a slower sorption process. However, since Fe30 has a higher iron concentration the overall chemisorption is the best in all the cases. Additionally, Figure 2-B shows the maximum weight increments of iron containing samples with a saturated CO_2 atmosphere (P_{CO2} = 1.0). As it could be expected, CO_2 capture was higher on saturated CO_2 atmosphere, in comparison to the weight increments obtained with a P_{CO2} = 0.2. Moreover, desorption temperatures were reduced using the low P_{CO2}. These results are in good agreement with the Le Châtelier equilibrium principle.

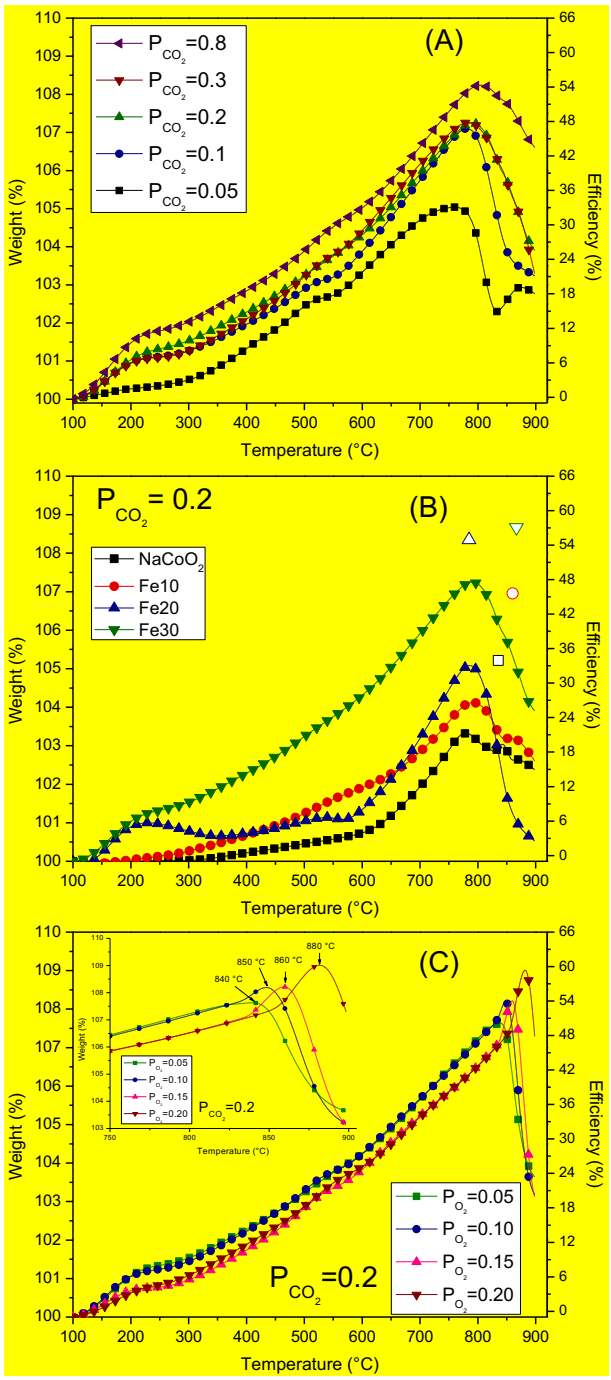

Figure 2. Dynamic TG analyses of Fe30-$NaCoO_2$ using different P_{CO2} (A), pristine $NaCoO_2$ and iron-containing samples using a P_{CO2} of 0.2 (B, independent labeled points correspond to maximum weight increments using a saturated CO_2 atmosphere) and Fe30-$NaCoO_2$ using a P_{CO2} of 0.2 and different P_{O2} (C). The maximum theoretic CO_2 chemisorption on $NaCoO_2$ is 115.2 wt%.

Then, the addition of oxygen into the feed stream was studied thermogravimetrically on Fe30 sample, using a P_{CO2} of 0.2 and varying P_{O2} between 0.05 and 0.2 (Figure 2-C). The most important changes were observed in the quantity of captured CO_2 as well as in shifts in temperature, compared to the experiments performed in oxygen absence. The highest CO_2 capture value was observed when using a P_{O2} of 0.2 (9.0 wt%), which is higher than the value obtained in oxygen absence, even under a saturated CO_2 flow (P_{CO2} = 0.8). While surface and bulk chemisorption processes remained at nearly the same temperature, the desorption process was shifted to higher temperatures compared to an atmosphere without oxygen, where desorption took place at 790 °C. In fact, desorption temperature increased linearly with the P_{O2}, varying from 840 to 880 °C for P_{O2} of 0.05 and 0.2, respectively (see square inset of Figure 2-C). To further analyze CO_2 capture at low partial pressures, different isothermal tests were performed (P_{CO2} = 0.2) in presence or absence of oxygen, between 500 and 800 °C, using two different P_{O2}; 0.05 and 0.2 (Figure 3). All these isotherms presented an exponential behavior and none of them reached the equilibrium after 3 hours. In oxygen absence, weight increased as a function of temperature going from 5.6 (efficiency, ε = 36.8 %, see equation 1) to 10.6 wt% (ε = 69.7 %) at 500 and 700 °C, respectively. However, at 800 °C the final weight decreased to 8 wt% (ε = 52.6 %). This behavior is in agreement with changes on the CO_2 chemisorption-desorption equilibrium, since at this temperature the desorption process has already begun (see Figure 2-A).

$$\varepsilon = \frac{100 \times W_G}{CO_2\ theoretical\ capacity} \quad (1)$$

where, W_G is the weight gained on each isotherm and *CO_2 theoretical capacity* of this specific process is 115.2 wt%; the maximum CO_2 that $NaCoO_2$ is able to trap in weight.

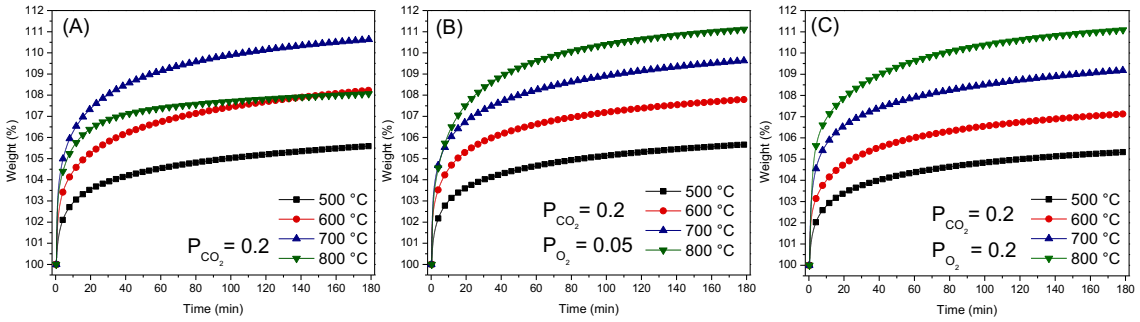

Figure 3. Thermogravimetric isothermal analyses of Fe30-$NaCoO_2$ samples at different temperatures, using different gas mixtures; P_{CO2} = 0.2 (A), P_{CO2} = 0.2 and P_{O2} = 0.05 (B) and P_{CO2} and P_{O2} equal to 0.2 (C). All the gas mixtures were N_2 balanced.

In oxygen presence, weight gains increased as a function of temperature as well, but in these cases CO_2 chemisorption trends were maintained over the whole temperature range (500-800 °C). Weight increments varied from 5.7 (ε = 37.5 %) at 500 °C to 11.1 wt% (ε = 73 %) at 800 °C using a P_{O2} = 0.05, while those increments varied from 5.3 (ε =34.8 %) to 11.1 wt% (ε =73 %) with an increased P_{O2} of 0.2. Furthermore, it can be observed that weight increments were slightly higher (~0.5 wt%) under a P_{O2} of 0.05 than those for P_{O2} of 0.2. It is also worth noting that according to these results, at T < 700 °C the final weight gains were always higher in absence of oxygen, indicating that oxygen addition into the stream is only beneficial at T > 700 °C. This behavior is opposite to that obtained when using saturated pressures of CO_2, where addition of oxygen leads to higher CO_2 captures (Vera et al. 2018). This finding might be due to the fact that when using similar partial pressures of CO_2 and O_2, oxygen may hinder or even compete for active sorption sites, reducing the overall CO_2 chemisorption. When P_{O2} is reduced (P_{O2} = 0.05 case), CO_2 capture improves with respect to P_{O2} = 0.2, but not enough to compensate its presence or even enhance the chemisorption. This is a similar behavior to that previously reported for Li_2ZrO_3, where a competition between CO_2 and O_2 for the active sorption sites was observed, resulting in a decrease in the

maximum CO_2 chemisorption as a function of the oxygen content. In this case, however, the difference is more noticeable as a low P_{CO2} is being used. Moreover, the general kinetic behavior presented by this process can be considered as good, due to the use of low P_{CO2}, which in other cases hinder the CO_2 capture efficiency and kinetics. Perhaps, the most clear example of this typical problem presented on alkaline ceramics is lithium orthosilicate (Li_4SiO_4, Oh-Ishi et al. 2014), which losses most of its CO_2 capture capacities by decreasing the CO_2 concentration.

To identify isothermal chemisorption products, some of them were characterized by XRD. Figure 4 shows the XRD patterns of isothermal products obtained at 700 and 800 °C with three different P_{O2}. At 700 °C and without oxygen, XRD pattern evidenced the formation of sodium carbonate (Na_2CO_3, 99-100-9289 PDF file), cobalt oxide (Co_3O_4, 03-065-3103 PDF file) and iron oxide (Fe_3O_4, 99-100-7425 PDF file), where both metal oxides have mixed oxidation states; 2+ and 3+. Additionally, when oxygen was added into the stream, the $Na_{0.74}CoO_2$ phase was still present, while in absence of oxygen it was no longer visible in the patterns. When temperature was increased to 800 °C, products included Na_2CO_3 and the same iron oxide (Fe_3O_4), although only the product evaluated with P_{O2} = 0.2 preserved the sodium cobaltate reflections. In absence of oxygen, a different cobalt oxide was produced: CoO (99-101-0489), indicating that cobalt is being reduced and consequently oxygen is released. According to these results, the addition of oxygen inhibits the gradual reduction of both Co and Fe, where they are re-oxidized by adsorbed gas-phase oxygen molecules. Moreover, it would seem that the increment of the P_{O2} hinders the pristine phase reactivity, even at high temperatures.

To further complement these analyses, data obtained from isothermal curves were fitted to the Jander-Zhang model (equation 2, (Zhang et al. 2017)). This model has been recently reported as adequate for low CO_2 partial pressures, where the reaction is considered to be kinetically controlled by mass diffusion.

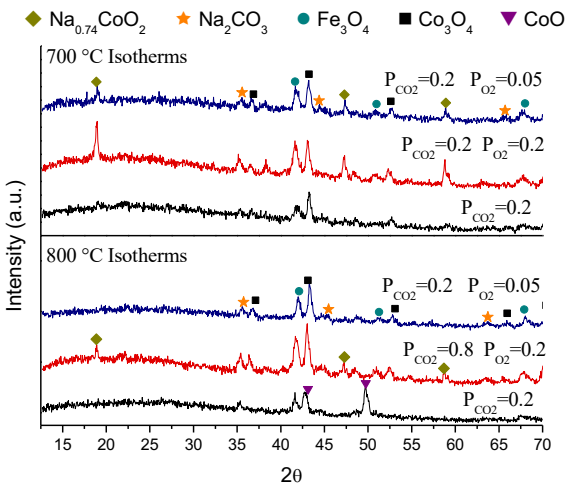

Figure 4. XRD patterns of isothermal products obtained at 700 and 800 °C with different P_{CO2} and P_{O2}.

$$\left(1-(1-Z\alpha)^{1/3}\right)^3 = k\left(P_{CO_2}\right)^{n_1} t \qquad (2)$$

where α is the conversion value of $NaCo_{0.7}Fe_{0.3}O_2$ (with respect to the maximum theoretical value of 15 wt%) at time t, Z is the proportion of Na_2CO_3 in the product shell, k is the rate constant (which depends on temperature), n_1 represents a kinetic parameter and P_{CO2} is the partial pressure used. According to the XRD results, Na_2CO_3 is formed along with Fe_3O_4 and Co_3O_4. In these cases, Z was adjusted to 0.5, which is the theoretical proportional part of Na_2CO_3 in all the products. However, when CoO was formed instead of Co_3O_4, Z was fixed to 0.3 (see reactions 3 and 4). Figure 5 shows the fitting results compared to the experimental conversion (α). It is observed that the calculated conversion curves are consistent with the experimental values, suggesting that this model accurately describes the CO_2 capture behavior at low partial pressures.

$$2\ Na_{0.74}Co_{0.7}Fe_{0.3}O_2 + 0.74\ CO_2 \rightarrow 0.74\ Na_2CO_3 + 0.46\ Co_3O_4 + 0.20\ Fe_3O_4 + 0.29\ O_2, \qquad Z = 0.53 \quad (3)$$

$$2\ Na_{0.74}Co_{0.7}Fe_{0.3}O_2 + 0.74\ CO_2 \xrightarrow{T \geq 800\ ^\circ C\ in\ O_2\ absence} 0.74\ Na_2CO_3 + 1.4\ CoO + 0.2\ Fe_3O_4 + 0.83\ O_2, \qquad Z = 0.32 \quad (4)$$

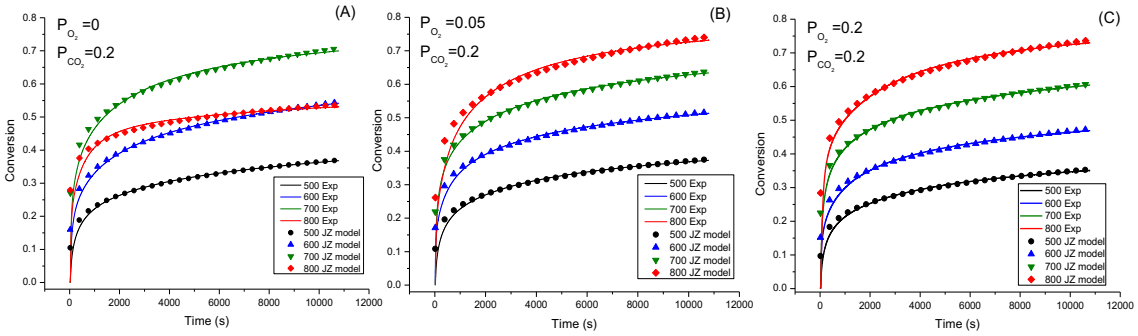

Figure 5. Experimental (lines) and fitted conversion values (points) using the Jander-Zhang model for the different gas mixtures; P_{CO2} = 0.2 (A), P_{CO2} = 0.2 and P_{O2} = 0.05 (B) and P_{CO2} and P_{O2} equal to 0.2 (C).

Table 1 shows the obtained *k* values for these three conditions. In all cases, values tended to increase as a function of temperature between 500 and 700 °C, varying from 8.9 x 10^{-7} to 2 x 10^{-5} s^{-1}, respectively and with higher values always for the P_{CO2} = 0.05 case. However, at 800 °C and in absence of oxygen, the rate constants diminished to 9.2 x 10^{-6} s^{-1}. In contrast, in oxygen presence, the rate constants either did not increase (P_{O2} = 0.05) or continued increasing (P = 0.2). These results suggest that even when the presence of oxygen hinders the CO_2 uptake of Fe-$NaCoO_2$ at low P_{CO2}, the CO_2 kinetics of the reaction is faster. This behavior is similar to that reported for Li_2CuO_2 or Li_2ZrO_3, where the carbonation process is kinetically favored by the presence of oxygen.

If the *k* values are compared to those obtained at saturated P_{CO2}, which lied between 1 x 10^{-4} and 7 x 10^{-3} s^{-1} (Vera et al. 2018), it can be seen that the values diminished in at least two orders of magnitude, which would be expected as kinetics of this reaction diminishes as a consequence of the low CO_2 concentration. When the *k* values are compared to those

obtained for other materials at low P_{CO2}, some differences are found. For example, the values obtained for Li_5AlO_4 using a P_{CO2} of 0.2 were between 0.2 and 1.1 x 10^{-3} s^{-1} under the best CO_2 capture conditions (700-750 °C) (Sánchez-Camacho et al. 2017), which are larger than the obtained for the Fe30-$NaCoO_2$. However, in the case of Li_4SiO_4 the *k* values were between 2 and 4 x 10^{-10} s^{-1} (575-625 °C) (Zhang et al. 2017), suggesting that at low P_{CO2} the kinetics of reaction are faster for the Fe30-$NaCoO_2$ than those of Li_4SiO_4.

Table 1. Rate constant values (*k*) obtained for $Na_{0.74}Co_{0.7}Fe_{0.3}O_2$ from Jander-Zhang modified model using different gas mixtures.

Temperature (°C)	P_{CO2} = 0.2 P_{O2} = 0		P_{CO2} = 0.2 P_{O2} = 0.05		P_{CO2} = 0.2 P_{O2} = 0.2	
	k (1/s)	R^2	k (1/s)	R^2	k (1/s)	R^2
500	8.9 x 10^{-7}	0.9975	1.1 x 10^{-6}	0.9956	9.2 x 10^{-7}	0.9955
600	3.1 x 10^{-6}	0.9975	6.5 x 10^{-6}	0.9943	3.9 x 10^{-6}	0.9942
700	2 x 10^{-5}	0.9916	2 x 10^{-5}	0.9958	2 x 10^{-5}	0.9957
800	9.2x10^{-6}	0.9638	2 x 10^{-5}	0.9847	3 x 10^{-5}	0.9924

Based on these results, the rate constant values were adjusted to Eyring's model (Figure 6), in order to obtain the activation enthalpy values ($\Delta H^{\ddagger}$). The following $\Delta H^{\ddagger}$ values were obtained 89.1, 76.8 and 61.7 kJ/mol for P_{O2} equal to 0.0 (absence of oxygen), 0.2 and 0.05, respectively. It must be mentioned that all these reactions correspond to endothermic processes. These results indicate that: *i*) the $\Delta H^{\ddagger}$ value (in absence of oxygen) increases from 17.9 to 89.1 kJ/mol when P_{CO2} is reduced from 1 and 0.2, suggesting that at low P_{CO2}, the reaction becomes more temperature dependent. *ii*) Contrary to saturated P_{CO2} conditions, the addition of O_2 into the stream yields reduced $\Delta H^{\ddagger}$ values in at least 12.3 kJ/mol, indicating that at low P_{CO2}, oxygen presence reduces the temperature dependence of this reaction. This behavior could be associated to the fact that the addition of O_2 improves the thermal stability

of the material. Moreover, it must be pointed out that the low data fitting may be correlated to the specific heat capacity variations presented in each temperature. The specific heat capacity changes as a function of the changing composition, described previously (see Figure 4).

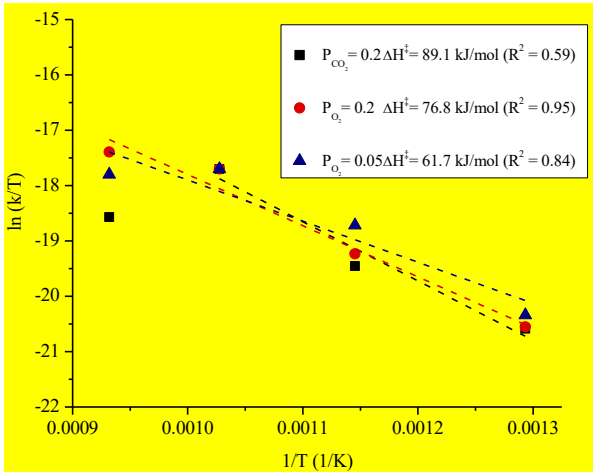

Figure 6. Eyring-type plot of ln (k/T) vs 1/T for the different P_{O2} (dashed lines) using the data obtained from the Jander-Zhang model (points).

3.3 CO-O_2 oxidation chemisorption analyses

In order to further analyze CO_2 capture from flue gases, it is also important to consider the effect on CO_2 capture of other components that may be present in the flue gas stream. Hence, the following systems were analyzed; CO-O_2, CO_2-CO and CO_2-CO-O_2, at low partial pressures (P_{CO} = 0.05, P_{CO2} = 0.03, P_{O2} = 0.03 or 0.05). Initially, CO oxidation and subsequent chemisorption were evaluated on Fe-$NaCoO_2$ samples (10, 20 and 30 mol% content) as well as in $NaCoO_2$, for comparison purposes. Figure 7-A shows the dynamic experiments performed in a catalytic reactor. CO conversion was observed even at room temperature, registering values between 10 to 30 % of conversion, which gradually decreased

to 0 % at 240 °C. This trend may be due to the reduction of iron or cobalt ions located on the surface, which may facilitate the CO oxidation at T < 200 °C by an easy oxygen release. At the particle surface, the availability of iron or cobalt ions is limited, explaining the gradual reduction of conversion. Above 240 °C, CO conversion increased continuously as a function of temperature until it reached 100 % of conversion. When using $NaCoO_2$, total conversion was achieved at 696 °C, and this temperature decreased as a function of Fe content to: 613, 571 and 530 °C for 10, 20 and 30 mol% content, respectively. Thus, Fe addition to $NaCoO_2$ shifts CO conversion to lower temperatures, as much as 166 °C when adding 30 mol% of Fe.

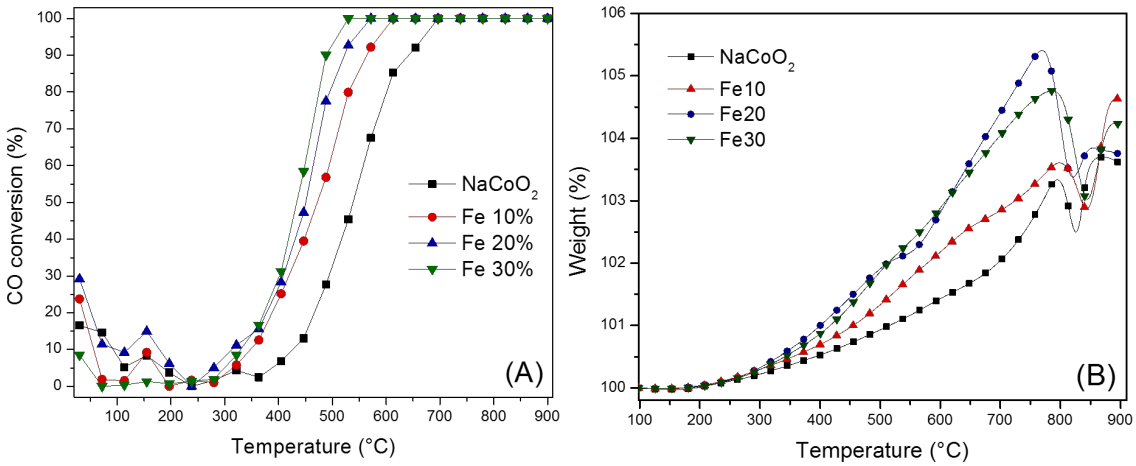

Figure 7. Dynamic thermal evolution of CO conversion (A) and TG curves (B) of CO-O_2 capture for pristine $NaCoO_2$ and iron-containing samples as catalyst-sorbents.

Subsequent chemisorption of CO_2 produced after CO oxidation was thermogravimetrically evaluated using the same conditions as in catalytic experiments (Figure 7-B). None of the analyzed samples presented weight increments below 200 °C. In contrast, when using a P_{CO2} = 0.05 (see Figure 2, which would be the closest result to the previous conditions used), CO_2 chemisorption began from 100 °C. However, the thermograms performed under the CO-O_2 mixture are in good agreement with the preceding CO catalytic experiment, where CO conversion began at around 240 °C. Above this

temperature, $NaCoO_2$, Fe10 and Fe30 samples presented a continuous weight increment up to decarbonation temperature: 790, 800 and 790 °C, respectively. On the other hand, for the Fe20 sample the weight increment could be more clearly divided in two stages: from 200 to 540 °C and from 540 to 770 °C, corresponding to superficial and bulk chemisorption, respectively. Overall, $NaCoO_2$ presented the lowest weight increment capturing up to 3.3 wt%, whilst Fe-containing samples presented higher weight increments at any temperature. Fe20 presented the highest weight increment (5.4 wt%), while Fe10 and Fe30 samples had weight gains of 3.6 and 4.7 wt%, respectively. These values are close to 5.1 wt% of Fe30 at a P_{CO2} of 0.05, suggesting that CO oxidation reaction on particle surface does not interfere with the CO_2 chemisorption on these materials.

Since Fe30 achieved the maximum CO conversion at the lowest temperature, further isothermal experiments between 300 and 800 °C were performed with that sample. Figure 8-A presents CO conversion values versus time for isothermal experiments conducted in the catalytic reactor. CO conversion increased from 23 to 93 % at 400 and 500 °C, respectively, remaining constant up to the end of each experiment. At 600, 700 and 800 °C CO conversion was 100 % during the whole experiment.

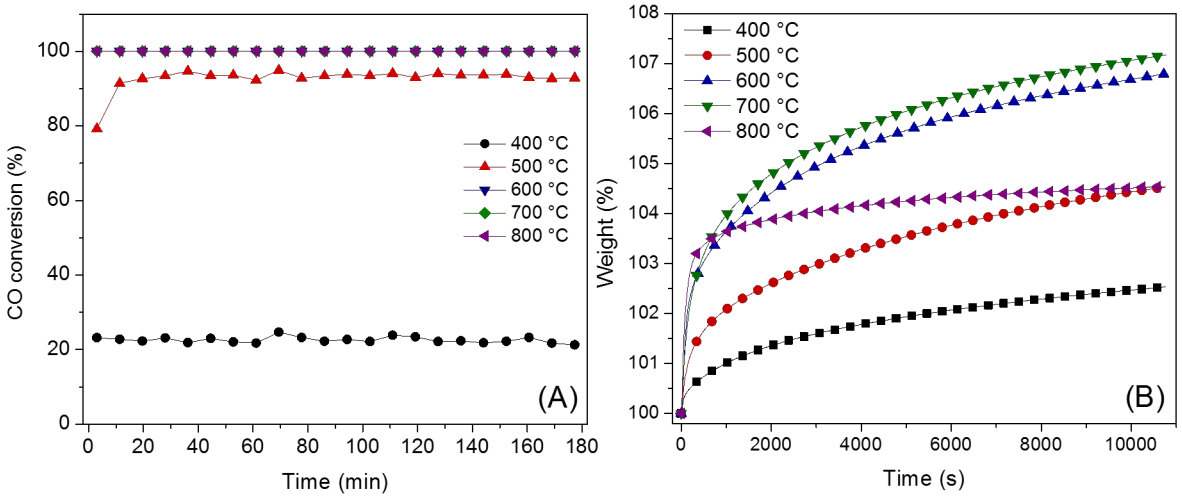

Figure 8. Isothermal evolution of CO conversion (A) and TG curves of CO capture for Fe30-$NaCoO_2$ (B).

Afterwards, the same isothermal analyses were performed in a thermogravimetric balance with the same conditions (Figure 8-B) to quantify the amount of produced CO_2 that was chemisorbed at each temperature. Between 400 and 700 °C curves presented an exponential behavior and none of them reached equilibrium after 3 hours. The final weight gains increased as a function of temperature from 2.5 to 7.2 wt% at 400 and 700 °C, respectively. While at short times, the weight gains tended to increase as a function of temperature, the capture uptake diminished dramatically at 800 °C, achieving a final capture of 4.5 wt%. This value corroborates the change on sorption-desorption equilibrium, i.e. at 800 °C the desorption process has already begun (Figure 7-B).

Figure 9 presents the XRD characterization of isothermal products from the catalytic reactor and pristine Fe30 sample pattern, for comparison purposes. At 300 and 400 °C, the only visible change is the reduction of intensities for all phases, namely $Na_{0.74}CoO_2$, $NaFeO_2$, Na_2CO_3 and FeO, which were also present in the products of the experiments carried out up to 800 °C but with a significant decrease in the intensity. Moreover, at 500 °C the XRD pattern exhibited the formation of Co_3O_4 (99-100-7004 PDF file) and Fe_3O_4 (99-100-6947 PDF file), whose intensities tended to increase (Co_3O_4) or remained (Fe_3O_4) constant at higher temperatures. Then, at 800 °C the formation of a different cobalt oxide phase (CoO, 01-072-1474 PDF file) phase was observed. According to these results, CO oxidation and its subsequent chemisorption produced the loss of crystallinity of pristine phase as a function of temperature. The formation of sodium carbonate as well as different crystalline phases of iron and cobalt oxides suggest that Fe30-$NaCoO_2$ sample must be carbonated as a result of CO_2 chemisorption. An interesting feature is the fact that $Na_{0.74}CoO_2$ phase is conserved even

at 800 °C for Fe30-$NaCoO_2$ sample, while in pristine $NaCoO_2$ this phase disappears at T ≥ 600 °C (Vera et al. 2016). Based on XRD results, iron oxidation state does not seem to be reduced and original FeO located at particle surface is conserved. This behavior prompts that Fe-$NaCoO_2$ samples follow a Mars van Krevelen-like reaction mechanism for the CO oxidation, where Fe and Co are the catalytic active species. Gas-phase oxygen molecules may be dissociated at the surface by Fe or Co, creating a surface layer of Fe-O or Co-O. Once oxygen reacts with CO, CO_2 is released from the surface leaving an anionic vacancy, which can be filled by either oxygen from the bulk or from the stream. In the case of Fe, this mechanism can proceed with an initial partial reduction of this cation (3+ to mixed 3+ and 2+) that remains constant even at high temperatures. Moreover, as most of iron is located at the material surface, it is easy to be re-oxidized. On the other hand, as Co is mainly located on bulk, Fe gradually reduces its oxidation state (3+ to 2+). By virtue of this, it seems that the presence of Fe in $NaCoO_2$ tends to stabilize the reduction rate of catalytic species, avoiding the deactivation of these materials. Based on these results, and in a previous report about the $NaCoO_2$ and Fe-$NaCoO_2$ carbonation-decarbonation processes [Vera et al. 2018], it can be assumed that cyclic processes can be achieved on these samples. In the previous report it was established that cyclic CO_2 sorption-desorption is favored on these samples when oxygen is added on the desorption process, as it re-oxidizes both transition metals, completing the crystal structure regeneration.

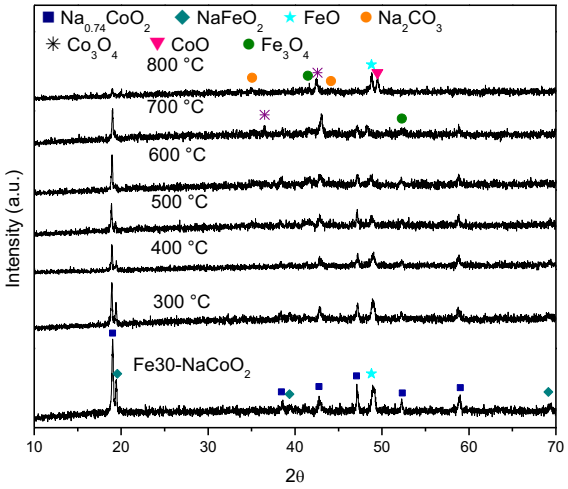

Figure 9. XRD patterns of isothermal products from the catalytic reactor and unreacted Fe30 sample pattern, for comparison purposes.

3.4 CO_2–CO selective chemisorption

After independent CO_2 and CO sorption and catalytic experiments, using low partial pressures, both carbon oxides were tested together (in absence or presence of O_2) on $NaCoO_2$ and Fe30-$NaCoO_2$ samples. These experiments were performed in order to analyze the gas sorption selectivity and mechanism on these samples. As in the CO analysis, different catalytic and thermogravimetric experiments were performed using CO-CO_2 or CO-CO_2-O_2 gas mixtures. Figure 10 shows the catalytic evolution and thermogravimetric analyses, using a CO-CO_2 gas mixture on pristine $NaCoO_2$ and Fe30-$NaCoO_2$. Gas evolution on the $NaCoO_2$-CO-CO_2 system clearly showed that CO is partially consumed between 280 and 500 °C, producing CO_2. Furthermore, in the same temperature range (280-500 °C), thermogravimetric analysis showed an important weight decrement (~6 wt%, Figure 8-C). Thus, $NaCoO_2$ must be catalyzing CO to CO_2, where oxygen atoms are being released from the $NaCoO_2$ crystal structure. Then, oxygen release must produce a cobalt partial reduction.

Based on that, CO_2 produced by the CO oxidation is not chemisorbed, as it was detected in the gas evolution as an excess. According to the stoichiometric relation needed for CO oxidation and the obtained experimental CO decrements, CO_2 increments between 300 and 450 °C should be higher. However, a small part of this produced CO_2 must be captured by the material, as it happens in Fe20-$NaCoO_2$ case. At temperatures higher than 500 °C, CO and CO_2 gas evolutions seemed to vary randomly, but corresponding thermogram showed a weight increment of 3.4 wt% between 640 and 780 °C. This weight increment might be related to the CO_2 chemical capture, coming from the CO oxidation and/or from the direct CO_2 capture, which is produced in this temperature range (see Figures 2 and 7). At T > 800 °C CO_2 concentration decreased, while CO was produced. This gravimetric and gas evolution trends indicate that a decarbonation process is taking place, where CO is produced and CO_2 tends to decrease. This could be associated to a partial CO_2 reduction towards CO caused as consequence of oxygen atoms being kept on the resultant solid phases previously reduced.

When the Fe30-$NaCoO_2$-CO-CO_2 system was used, although gas evolution was similar to pristine $NaCoO_2$ case at temperatures lower than 600 °C, thermogravimetric analysis was completely different. CO was almost totally consumed between 350 and 500 °C, producing CO_2. However, in this case, Fe30 sample did not lose weight (Figure 10-C), as in the pristine $NaCoO_2$ case. Here, Fe30 sample gained around 1 wt%. Thus, superficial iron oxide must be reduced producing CO_2, which was subsequently chemisorbed on $NaCoO_2$, as it is presented in reaction 5.

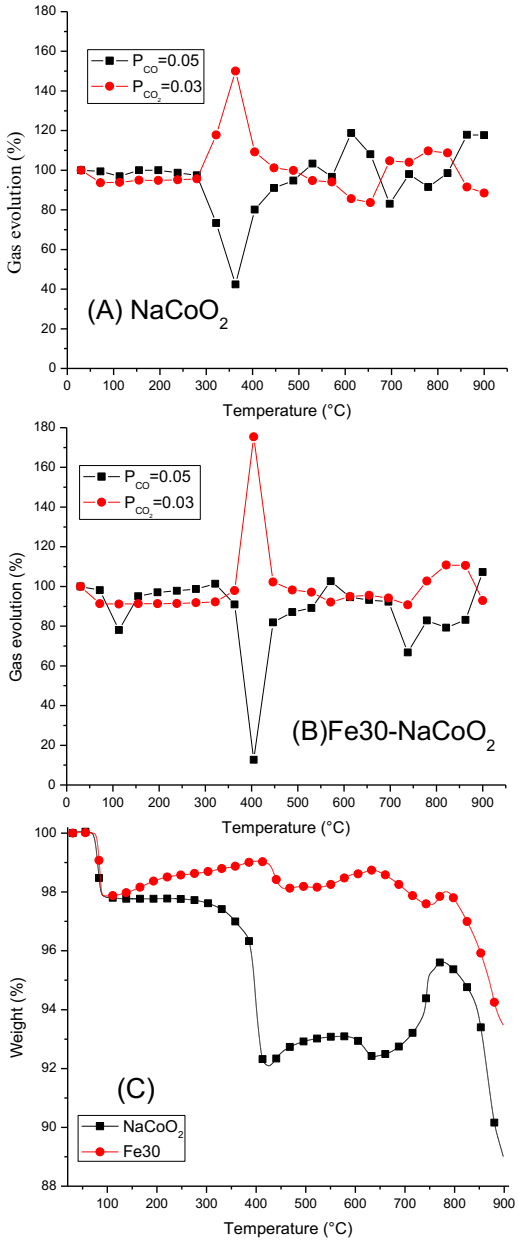

Figure 10. Catalytic evolution of CO and CO_2 using pristine $NaCoO_2$ (A) and Fe30-$NaCoO_2$ (B), as well as dynamic thermogravimetric profile (C) of both samples.

$$2NaCoO_2 + FeO \xrightarrow{CO} 2NaCoO_2 + Fe \xrightarrow{CO_2} Na_2CO_3 + Co_2O_3 + Fe \qquad (5)$$

Based on that, it is evident that iron addition favors CO oxidation and chemisorption. This observation may be explained based on the Fe and Co reduction potentials; Fe (2+ →

0, 0.44 V) > Co (3+ → 0, 0.28 V), considering that Co^{3+} (3+ → 2+, -0.1 V) has even a lower reduction potential. According to these values, Fe has a greater tendency to be reduced than Co, hence it is easier for the Fe30-$NaCoO_2$ to donate lattice oxygen anions for the CO oxidation, than for the pristine $NaCoO_2$, leading to a higher CO_2 production. As it could be expected, adding oxygen to the gas mixture totally changed the sorption and catalytic behaviors of both samples (Figure 11). Both samples presented the CO oxidation process within the same temperature range, beginning at 360 °C and reaching a total conversion at around 560-600 °C. Correspondingly, CO_2 production was importantly high in both systems, reaching detection percentages of more than 220 %, while oxygen consumption was equal to 78 and 89 % for pristine $NaCoO_2$ and Fe30-$NaCoO_2$ samples, respectively. At the same time, thermogravimetric curves (Figure 11-C) showed weight gains on both cases, and the Fe30-$NaCoO_2$ sample always presented higher increments than pristine $NaCoO_2$ between 100 and 830 °C. Weight decrements observed at $T \leq 100$ °C simply correspond to a dehydration process. These results showed that, in oxygen presence, both ceramics are able to perform the CO oxidation without any important variations, but the iron-containing sample presents a higher CO_2 capture. It may be postulated that iron facilitates oxygen dissociation for the CO_2 and carbonate formation, through the Mars van Krevelen (1954) reaction mechanism.

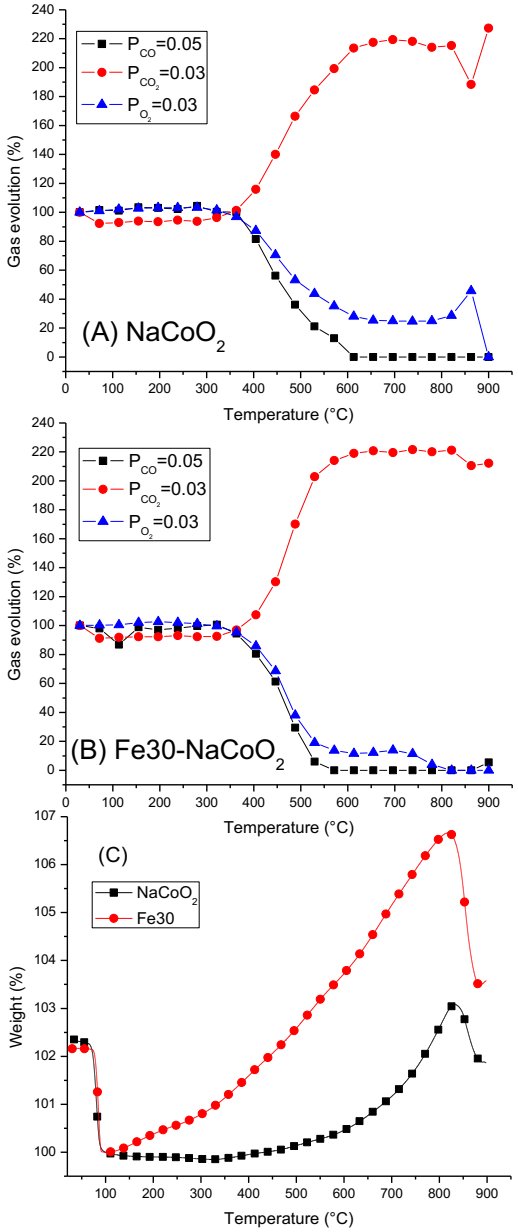

Figure 11. Catalytic evolution of CO, CO_2 and O_2 using pristine $NaCoO_2$ (A) and Fe30-$NaCoO_2$ (B), as well as dynamic thermogravimetric profile (C) of both samples.

Conclusions

The CO_2 chemisorption results, on pristine and Fe-containing $NaCoO_2$ samples, indicated that for $P_{CO2} \geq 0.1$ CO_2 chemisorption was not significantly reduced. This result

suggests that $NaCoO_2$ could be used in some combustion flows, with similar P_{CO2} as energy requirements for the material regeneration would be lesser. Moreover, Fe-containing $NaCoO_2$ samples clearly showed that iron addition improved the CO_2 chemisorption efficiency, even at the lowest P_{CO2}. It was explained by the partial iron reduction from Fe^{3+} to Fe^{2+} or Fe^0, implying that iron oxides were able to release oxygen. Furthermore, when oxygen was added to the gas flow the chemisorption process was improved, as iron atoms presented a continuous reduction-oxidation mechanism. These results were kinetically analyzed by the Jander-Zhang and Eyring models. After the analyses performed in CO_2 and CO_2-O_2 flows systems, the effect produced by CO addition was studied. CO conversion was observed over a broad temperature range (240-900 °C), which was linked to iron reduction and simultaneous oxygen release. However, CO oxidation and chemisorption were reduced as a function of the iron availability. Finally, simultaneous CO_2 and CO sorption and catalytic experiments were conducted (in absence or presence of O_2), on pristine and Fe30-$NaCoO_2$ samples. Gas evolution on the $NaCoO_2$-CO-CO_2 system clearly showed that CO was partially consumed producing CO_2 (280 and 500 °C), while thermogravimetric analysis showed an important weight decrement (~6 wt%). Thus, $NaCoO_2$ catalyzed CO to CO_2, where oxygen atoms are being released from the $NaCoO_2$ crystal structure. At T > 500 °C, while CO and CO_2 gas evolutions seemed to vary randomly, the corresponding thermogram showed a weight increment corresponding to CO_2 chemical capture. Fe30-$NaCoO_2$-CO-CO_2 presented a different behavior than pristine $NaCoO_2$ at high temperatures. In that case, CO was almost consumed between 350 and 500 °C, producing CO_2, but this sample did not lose weight. Thus, superficial iron oxide must be reduced producing CO_2, which was subsequently chemisorbed on $NaCoO_2$.

Acknowledgements

E. Vera thanks to CONACYT for personal financial supports. This work was financially supported by projects SENER-CONACYT (251801) and PAPIIT-UNAM (IN-201419). Authors thank to Adriana Tejeda and Omar Novelo for technical assistant.

References

Alcántar-Vázquez, B., Duan, Y., Pfeiffer, H., CO oxidation and Subsequent CO_2 chemisorption on Alkaline Zirconates: Li_2ZrO_3 and Na_2ZrO_3, Ind. Eng. Chem. Res. 55, 9880–9886 (2016).

Bhatta, L. K. G., Subramanyam, S., Chengala, M. D., Olivera, S., Venkatesh, K., Progress in hydrotalcite like compounds and metal-based oxides for CO_2 capture: a review, J. Cleaner Prod. 103, 171−196 (2015).

Chowdhury, M. B. I., Quddus, M. R., de Lasa, H. I., CO_2 capture with a novel solid fluidizable sorbent: Thermodynamics and Temperature Programmed Carbonation-Decarbonation, Chem. Eng. J. 232, 139–148 (2013).

Dou, B., Wang, C., Song, Y., Chen, H., Jiang, B., Yang, M., Xu, Y., Solid sorbents for in-situ CO_2 removal during sorption-enhanced steam reforming process: A review, Renew. Sustain. Energy Rev. 53, 536–546 (2016).

Izquierdo, M. T., Saleh, A., Sánchez-Fernández, E., Maroto-Valer, M. M., García, S., High-temperature CO_2 capture by Li_4SiO_4 sorbents: Effect of CO_2 concentration and cyclic

performance under representative conditions, Ind. Eng. Chem. Res. 57, 13802–13810 (2018).

Izquierdo, M. T., Turan, A., García, S. Maroto-Valer, M. M. Optimization of Li_4SiO_4 synthesis conditions by solid state method for maximum CO_2 capture at high temperature, J. Mat. Chem. A, 6, 3249–3257 (2018).

Kaniwa, S., Yoshino, M., Niwa, E., Yashima, M., Hashimoto, T., Analysis of chemical reaction between Li_4SiO_4 and CO_2 by thermogravimetry under various CO_2 partial pressures—Clarification of CO_2 partial pressure and temperature region of CO_2 absorption or desorption, Mater. Res. Bull. 94, 134–139 (2017).

Kaniwa, S., Yoshino, M., Niwa, E., Hashimoto, T., Evaluation of reaction kinetics of CO_2 and Li_4SiO_4 by thermogravimetry under various CO_2 partial pressures, Mater. Res. Bull. 97, 56–60 (2018).

Kenarsari, S. D. Yang, D., Jiang, G., Zhang, S., Wang, J., Russell, A. G., Wei, Q., Fan M., Review of recent advances in carbon dioxide separation and capture, RSC Adv. 3, 22739−22773 (2013).

Lara-García, H. A., Vera, E., Mendoza-Nieto, J. A., Gomez-García, J. F., Duan, Y., Pfeiffer, H., Bifunctional application of lithium ferrites (Li_5FeO_4 and $LiFeO_2$) during carbon monoxide (CO) oxidation and chemisorption processes. A catalytic, thermogravimetric and theoretical analysis, Chem. Eng. J., 327, 783–791 (2017).

Lara-García, H. A., Pfeiffer, H., High and efficient Li_2CuO_2-CO_2 chemisorption using different partial pressures and enhancement produced by the oxygen addition, Chem. Eng. J. 313, 1288–1294 (2017).

Mars, P., van-Krevelen, D. W., Oxidations carried out by means of vanadium oxide catalysts. Chem. Eng. Sci. 3, 41−59 (1954).

Ochoa-Fernández, E.; Zhao, T.; Rønning, M.; Chen, D. Effects of steam addition on the properties of high temperature ceramic CO_2 acceptors. J. Environ. Eng. 135, 397–403 (2009).

Oh-Ishi, K., Matsukura, Y., Okumura, T., Matsunaga, Y., Kobayashi, R., Fundamental research on gas–solid reaction between CO_2 and Li_2CuO_2 linking application for solid CO_2 absorbent, J. Solid State Chem. 211, 162–169 (2014).

Regufe, M. J., Ferreira, A. F. P., Loureiro, J. M., Shi, Y., Rodrigues, A., Ribeiro, A. M., New hybrid composite honeycomb monolith with 13X zeolite and activated carbon for CO_2 capture, Ads. 24, 249−265 (2018).

Sánchez-Camacho, P., Gómez-García, J. F., Pfeiffer, H., Thermokinetic and conductivity analyzes of the high CO_2 chemisorption on Li_5AlO_4 and alkaline carbonate impregnated Li_5AlO_4 samples: Effects produced by the use of CO_2 partial pressures and, oxygen addition, J. Energy Chem. 26, 919–926 (2017).

Stonor, M. R., Ferguson, T. E., Chen, J. G., Park, A. H. A., Biomass conversion to H_2 with substantially suppressed CO_2 formation in the presence of group I & group II hydroxides and a Ni/ZrO_2 catalyst, Energy Environ. Sci. 8, 1702–1706 (2015).

Vera, E., Alcantar-Vazquez, B., Pfeiffer, H., CO_2 chemisorption and evidence of the CO oxidation–chemisorption mechanisms on sodium cobaltate, Chem. Eng. J. 271, 106–113 (2015).

Vera, E., Alcántar-Vázquez, B., Duan, Y., Pfeiffer, H., Bifunctional application of sodium cobaltate as a catalyst and captor through CO oxidation and subsequent CO_2 chemisorption processes, RSC Adv., 6, 2162−2170 (2016).

Vera, E., Gomez-García, J. F., Pfeiffer, H., Enhanced CO_2 chemisorption at high temperatures via oxygen addition using (Fe, Cu or Ni)-containing sodium cobaltates as solid sorbents, J. CO_2 Util. 25, 147−157 (2018).

Wai, L. T., Jeng, S. L., Haslenda, H., Azizul, M. A., Wai, S. H., Shin, H., Review of pre-combustion capture and ionic liquid in carbon capture and storage, Appl. Energy 183, 1633–1663 (2016).

Wang, J., Huang, L., Yang, R., Zhang, Z., Wu, J., Gao, Y., Wang, Q., O'Hare, O., Zhong, Z., Recent advances in solid sorbents for CO_2 capture and new development trends Energy Environ. Sci., 7, 3478−3518 (2014).

Webley, P. A., Adsorption technology for CO_2 separation and capture: a perspective, Ads. 20, 225−231 (2014).

Yañez-Aulestia, A., Gómez-García, J. F., Mendoza-Nieto, J. A., Duan, Y., Pfeiffer, H., Thermocatalytic analysis of CO_2-CO selective chemisorption mechanism on lithium cuprate (Li_2CuO_2) and oxygen addition effect, Thermochim. Acta 660, 144-151 (2018).

Zhang, Q., Peng, D., Zhang, S., Ye, Q., Wu, Y., Ni, Y., Behaviors and kinetic models analysis of Li_4SiO_4 under various CO_2 partial pressures, AIChE J. 63, 2153−2164 (2017).

Zhang, Y., Yu, F., Louis, B., Wang, Q., Stable synthesis of the lithium silicate-based high-temperature CO_2 sorbent from inexpensive raw material vermiculite, Chem. Eng. J. 349, 562−573 (2018).

Zhang, Y., Gao, Y., Pfeiffer, H., Louis, B., Sun, L., O' Hare, D., Wang, Q., Recent advances in lithium containing ceramic based sorbents for high-temperature CO_2 capture J. Mater. Chem. A, 7, 7962–8005 (2019).

Zhao, M., Fan, H., Song, Y., He, X., Memon, M. Z., Bathia, S. K., Ji, G., Kinetic analysis for cyclic CO_2 capture using lithium orthosilicate sorbents derived from different silicon precursors, Dalton Trans. 47, 9038–9050 (2018).

CO_2-CO capture and kinetic analyses of sodium cobaltate under various partial pressures

Elizabeth Vera,[1,2] Susana García,[2] M. Mercedes Maroto-Valer,[2] and Heriberto Pfeiffer[1,*]

[1]*Laboratorio de Fisicoquímica y Reactividad de Superficies (LaFReS), Instituto de Investigaciones en Materiales, Universidad Nacional Autónoma de México, Circuito exterior s/n, Ciudad Universitaria, Del. Coyoacán C.P. 04510, Ciudad de México, Mexico.*

[2]*Research Centre for Carbon Solutions (RCCS), Heriot-Watt University, Edinburgh, EH14 4AS, United Kingdom.*

**Corresponding author. Phone +52 (55) 5622 4627, fax +52 (55) 5616 1371 and E-mail pfeiffer@materiales.unam.mx*

Supplementary Information

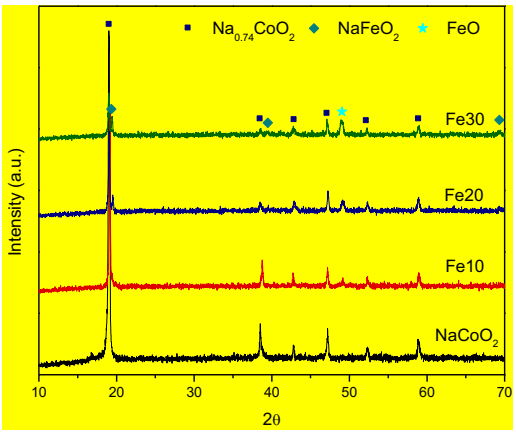

Figure S1. XRD patterns of the pristine and Fe-containing $NaCoO_2$ samples with 10, 20 and 30 mol% of iron. All these patterns were identified with the $Na_{0.74}CoO_2$ crystalline phase, where Fe-$NaCoO_2$ samples presented small amounts of $NaFeO_2$ and FeO phases.